SIMPLIFIED MODEL FOR LARGE MASS IMPACT AND DELAMINATION ONSET IN CURVED LAMINATES

Robin Olsson

Imperial College, Department of Aeronautics
London, SW7 2AZ, UK
r.olsson@imperial.ac.uk

ABSTRACT

The current paper presents a simplified closed form approach to predict impact response and delamination onset in laminated composite cylinders and curved panels under large mass impact. The approach assumes a quasi-static impact response and the mass conditions for this type of response are stated. Available static solutions for long and short cylinders are reviewed and their range of validity discussed. A simplified approach to consider large deflections and indentation is suggested. Finally the predictions are compared with two published impact experiments with composite cylinders and one with a shallow curved panel. The predictions of the initial response and delamination onset are in good agreement with experiments, but the large deflection effects in the curved panel are not fully captured.

1. INTRODUCTION

Impact resistance and damage tolerance remain major concerns in the design of laminated composite structures. Flat and almost flat laminates are used in a number of applications, but curved laminates are unavoidable in wind turbine blades, aircraft fuselages, wing skins, and in the bodies of most other vehicles. Cylindrical composite tubes are also finding increasing use in the oil and offshore industry. Impact on flat panels has been the subject of extensive experimental and theoretical studies [1], while the work on curved panels is more limited [2]. Examples of combined theoretical and experimental work on large mass impact on cylinders can be found in [3-7].

The existence of a delamination threshold load for flat panels has been demonstrated earlier [8], and experiments indicate that it also is applicable for curved panels [7]. Thus, methods are needed to predict the peak load during impact on curved panels.

Most numerical solutions for curved panels have addressed short time impacts with a local wave controlled response caused by relatively small impactors, while experiments usually involve impact by relatively heavy impactors. Heavy impactors cause a quasi-static response which can be modelled using static solutions for a point load at the impact location, Fig. 1. A requirement is that the impactor mass M is much larger than the dynamic mass M_s^* of the part of the shell which is affected by the impact.

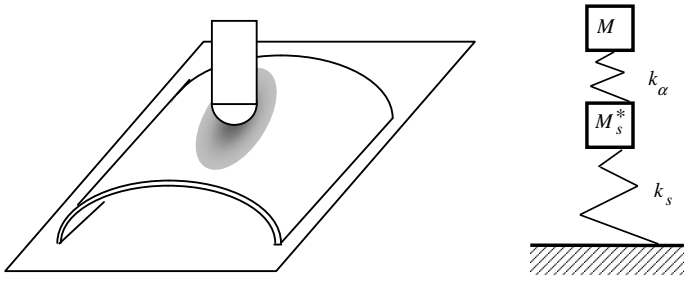

Figure 1: Simplified model for impact on curved panel.

Several analytical solutions have been presented for impact on cylinders, but predictions are generally obtained from stepwise solution of equations involving infinite series rather than from explicit expressions for the peak load. The present paper addresses available solutions for a concentrated static load on curved and cylindrical panels, and explains how they can be used to predict the peak load and delamination onset during impact on curved laminates.

2. FLEXIBILITY OF LONG CYLINDER

It is useful to first consider the solution for an infinite ($L/a>>1$) isotropic cylinder under the action of two diametrically opposed radial loads F, Fig. 2.

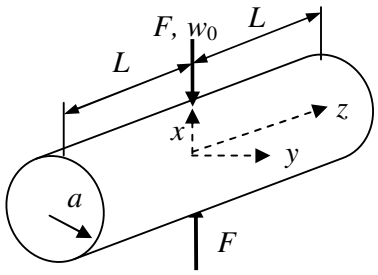

Figure 2: Geometry of cylinder.

Solutions have been derived using Flügge's equations [9], the complete Donnel equations [10] and Morley's equations [11]. A more complete list of relevant work may be found in [2]. A particularly simple and convenient approximation was presented in [10]. Here we will consider the extension of this solution to orthotropic shells suggested in [12], where the deflection w_∞ of an infinitely long cylinder is given by:

$$w_\infty(z,s) = FC_{0\infty} =$$

$$2F\kappa^3/\left(\pi E_z h H^3\right)\sum_{m=2,4..}^{m<\kappa} m^{-2}\left(1-1/m^2\right)^{-3/2}\left[\cos\left(H\mu_m\bar{z}\right)+\sin\left(H\mu_m\bar{z}\right)\right]e^{-H\mu_m\bar{z}}\cos\left(ns/a\right) \quad (1)$$

$$\text{where } H^4 = E_\theta/E_z \qquad \bar{z} = z/a \qquad \kappa^4 = 3\left(1-\nu_{z\theta}\nu_{\theta z}\right)(a/h)^2 \qquad \mu_n = \tfrac{1}{2}m\left(m^2-1\right)/\kappa$$

The expression given in [12] has been corrected for typesetting errors by redefining H and moving one κ from the denominator to the nominator (confirmed with the author of [12]). For convenience we replace the even indices m=2,4,6 etc used in [10, 12] by $2n$ (n=1,2,3 etc) and rewrite the equation on the following form

$$w_\infty(z,\theta) = \psi_\infty\left(1-\nu_{z\theta}\nu_{\theta z}\right)^{3/4} F(a/h)^{3/2} H/\left(E_\theta h\right) \qquad \text{where}$$

$$\psi_\infty(\zeta,\theta) = 3^{3/4}\frac{4}{\pi}\sum_{n=1}^{n<\kappa} n\left(4n^2-1\right)^{-3/2}\left[\cos\left(\mu_n\zeta\right)+\sin\left(\mu_n\zeta\right)\right]e^{-\mu_n\zeta}\cos\left(2n\theta\right) \quad (2)$$

$$\text{and } H^4 = E_\theta/E_z \qquad \zeta = H\,z/a \qquad \kappa^4 = 3\left(1-\nu_{z\theta}\nu_{\theta z}\right)(a/h)^2 \quad \mu_n = n\left(4n^2-1\right)/\kappa$$

This is a rapidly converging series, and good results are obtained with just a few terms. Note that the series should be terminated for $n<\kappa$. The quantity κ is a measure of how thin the shell is, and is a key parameter in shell equations. The quantity H is effectively a length scaling parameter, familiar from equations for orthotropic plates.

Thus, for an infinitely long *full cylinder* the functions ψ_0 at the point of load application and ψ_{90} at 90º in the same cross section are given by:

$$\begin{aligned}\psi_0 = \psi_\infty(0,0) \quad &= 3^{3/4}\,\tfrac{4}{\pi}\textstyle\sum_{n=1}^{n<\kappa} n \,/\left(4n^2-1\right)^{3/2} \quad \approx \; 0.800 \\ \psi_{90} = \psi_\infty(0,\pi/2) &= 3^{3/4}\,\tfrac{4}{\pi}\textstyle\sum_{n=1}^{n<\kappa}(-1)^n n/\left(4n^2-1\right)^{3/2} \approx -0.486\end{aligned} \tag{3}$$

The deflection of a *half cylinder with rigidly clamped edges* may be obtained by superimposing the deformation of an inextensible cylinder deformed to an ellipse with displacements $-w_\infty(z,\pi/2)$ along the axial edges and displacements $+w_\infty(z,\pi/2)$ along θ=0. Only even terms $2n$ in the series are retained. Thus, the function ψ at the point of load application in the rigidly clamped half cylinder is:

$$\psi_{\infty C/2}(0,0) = 3^{3/4}\,\tfrac{8}{\pi}\textstyle\sum_{n=1}^{n<\kappa} 2n \,/\left(16n^2-1\right)^{3/2} \approx 0.314 \tag{4}$$

The characteristic decay length in the axial direction is given by the leading terms in Eq. (2):

$$\begin{aligned}&w \propto\sim w_0 e^{-\mu_n H z/a} = w_0 e^{-z/L_z} \qquad \text{where} \\ &L_{zF} = a/(\mu_1 H) = a\kappa/(3H) = a\sqrt{a/h}\cdot\left[(1-\nu_{z\theta}\nu_{\theta z})E_z/E_\theta\right]^{1/4}/3^{3/4} \text{ for full cylinder} \\ &L_{zC/2} = a/(\mu_2 H) = a\kappa/(30H) = L_{zF}/10 \qquad \text{for rigidly clamped half - cylinder}\end{aligned} \tag{5}$$

Thus, the decay of deflections in isotropic thin walled (a/h>>1) full cylinders is much slower in the axial direction than in the circumferential direction, where the decay length is of the order of a. The decay length for the rigidly clamped half-cylinder indicates that the decay rate in cylinder segments with fixed edges is an order of magnitude larger than in full cylinders. In orthotropic cylinders the axial decay length increases with increasing axial stiffness, and ratio between the effective length L^* and true length L of orthotropic cylinders is given by:

$$L^* = HL = (E_\theta/E_z)^{1/4} L \tag{6}$$

Corrections for finite length cylinders were presented in [10] and can be written on the following format:

$$\begin{aligned}&w_F = w(0,0) = FC_0 = (\psi_0 + \psi_{end})(1-\nu_{z\theta}\nu_{\theta z})^{3/4}\, F(a/h)^{3/2} H/(E_\theta h) \\ &\text{where} \quad \psi_{end} = 3^{3/4}\,\tfrac{4}{\pi}\textstyle\sum_{n=1}^{n<\kappa} J_n n \,/\left(4n^2-1\right)^{3/2}\end{aligned} \tag{7}$$

Using the scaling factor in Eq. (6) the correction factor J_n for a central load on a cylinder with *free ends* may be written as follows:

$$J_n = \frac{2+\cos\left(2\mu_n L^*/a\right) - \sin\left(2\mu_n L^*/a\right) + e^{-2\mu_n L^*/a}}{1+2e^{-2\mu_n L^*/a}\sin\left(2\mu_n L^*/a\right) + e^{-4\mu_n L^*/a}}\, 2e^{-2\mu_n L^*/a} \tag{8}$$

The correction factors provided in [10] are based on the assumption that L^*/a is at least in the order of unity. For short cylinders with free ends solutions for curved beams are more appropriate.

3. FLEXIBILITY OF SHORT CYLINDER WITH FREE ENDS

Sufficiently short cylinders with free ends can be modeled as curved plates undergoing cylindrical bending (κ_z<<κ_θ) and solutions may be obtained from the solutions for curved beams, by replacing EI by $2LD_\theta$. We will assume the shell is thin, i.e. $(h/a)^2$<<1.

Due to symmetry only half the shell needs to be modeled. A general case of a curved beam is shown in Fig. 3.

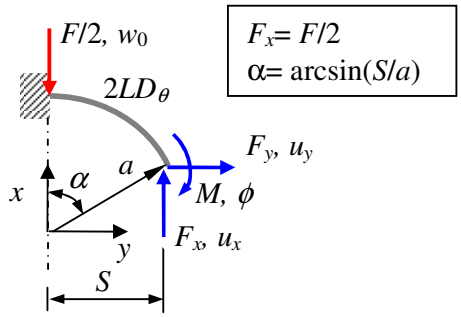

Figure 3: Loading of curved beam.

By combining the general solutions provided in [13] and satisfying the boundary conditions we obtain the following solutions:

3.1 Clamped sliding edges (ϕ=F_y=0)

$$w_C = FC_C = \frac{Fa^3}{8 \cdot 2LD_\theta}\left[4\alpha + 3\sin 2\alpha - 2\alpha\cos 2\alpha - 8\sin\alpha - 4(\alpha\sin\alpha + \cos\alpha - 1)^2/\alpha\right] \quad (9)$$

When α=π/2 this solution is applicable to a tubular ring under two diametrically opposed radial loads, as no shear forces F_y develop on symmetry planes. The solution then simplifies to:

$$w_R = FC_R = \frac{Fa^3}{\pi 2LD_\theta}\left[\pi^2/8 - 1\right] \quad (10)$$

Interestingly this simple closed form solution is numerically identical to the fairly complex Rayleigh energy solution derived by Timoshenko [14].

3.2 Pinned edges (u_y=M=0)

$$w_P = FC_P = -u_x =$$

$$\frac{Fa^3}{8 \cdot 2LD_\theta}\left[4\alpha + 3\sin 2\alpha - 2\alpha\cos 2\alpha - 8\sin\alpha + 2\tilde{F}_y(4\cos\alpha - 3\cos 2\alpha - 2\alpha\sin 2\alpha - 1)\right] \quad (11)$$

where $\tilde{F}_y = F_y/F = -(4\cos\alpha - 3\cos 2\alpha - 2\alpha\sin 2\alpha - 1)/(4\alpha + 2\alpha\cos 2\alpha - 3\sin 2\alpha)$

For a half cylinder (α=π/2) the solution simplifies to:

$$w_P = FC_{P90} = \frac{Fa^3}{8 \cdot 2LD_\theta}\left[3\pi - 8 - 4/\pi\right] \quad (12)$$

4. EFFECT OF LARGE DEFLECTIONS AND INDENTATION

4.1 Large local deflection of shells

Deflections exceeding the thickness of the shell are common during impact and generate membrane stresses which have a significant influence on the response. For flat plates and concave shells the curvature is increasing with increasing deflection, which increases the stiffness of the structure. In contrast deflection of convex shells causes a decreasing curvature and a reduced stiffness of the structure.

A qualitative account of the effects of large local deflections in convex cylinders can be made by considering an approximate solution for convex paraboloidal shells [15]. The

approach is based on the observation that the membrane deformation of thin shells is negligible in comparison to the bending deformation. Thus, the large local deflections of a shell must result in a dimple with a shape which essentially is a mirror image of the original convex shape. The deflection w_D from the original shape was found by equating the bending strain energy of the dimple and the work done during deflection. Strictly the expression is not valid for a cylinder as the initial radius of curvature is infinite in the axial direction while the aspect ratio of the dimple half axes is finite. However, considering that the curvature in the axial direction will be negligible the dimple deflection of a cylinder can be approximated by setting one of the two curvatures for the paraboloid surface to zero, which gives the following expression:

$$w_D = FC_D = \frac{4F^2a^2}{9\pi^2\chi^2 E_z E_\theta h^5} \quad \text{where} \quad \chi \approx 0.19 \tag{13}$$

The expression in [15] has been modified by substituting E_zE_θ for E^2 while χ is a constant derived in [15].

4.2 Large global deflection of short shells

Short curved shells may be approximated as curved beams (arches). It is known that shallow arches (α<30º or S/a<1/2 in Fig. 3) show significant geometrical nonlinearity which eventually leads to snap-through. Large deflections in a pinned shallow arch were examined in [16], where the rise of the arch was expressed as y_0 in the unloaded state and y in the loaded state. By substituting the symbols used in [16] by those of the present paper (y_0–$y \rightarrow w_P$; $R \rightarrow a$; $Q \rightarrow -F_y$; $P \rightarrow F/2$; $\mu \rightarrow q$ and $EI \rightarrow 2LD_\theta$) the solution in [16] can be written:

$$w = \frac{S^2}{2a} + \frac{2LD_\theta}{F_y a}\left[1/\cos(qS) - 1\right] - \frac{F}{2F_y}\left[\tan(qS)/q - S\right] \quad \text{where} \quad q^2 = -F_y/(2LD_\theta) \tag{14}$$

A first order approximation to this equation may be obtained by using the relation between the forces F_y and F obtained from the linear solution in Eq. (11).

4.3 Local indentation of the shell wall

An additional source of compliance is the indentation of the shell, i.e. the local thickness reduction, which approximately is given by the following expression [8]:

$$\begin{aligned} &w_\alpha = (F/k_\alpha)^{2/3} \quad \text{with} \quad k_\alpha \approx \tfrac{4}{3} Q_\alpha \sqrt{R} \\ &\text{where} \quad 1/Q_\alpha = 1/Q_{zi} + 1/Q_{zs} \quad \text{and} \quad 1/Q_z = (1 - \nu_{rz}\nu_{zr})/E_z \end{aligned} \tag{15}$$

Here R is the impactor tup radius and Q_{zi} and Q_{zs} are the effective out-of-plane moduli of the impactor and shell. Strictly, corrections of Eq. (15) are needed for finite thickness and large deflections, but in practice they can be neglected as the influence of indentation only is of importance for fairly thick shells and small deflections.

5. MASS CONDITION FOR QUASI-STATIC IMPACT RESPONSE

If the dynamic mass M_s^* of the impacted cylindrical shell is small in comparison to the impactor mass the impact may be described by a one degree-of-freedom model, involving the impactor mass M and the compliance C, which is the inverse of the stiffness k at the point of impact. For a quasi-static impact on a short floor-supported cylinder, Fig. 4a, the displacement at the point of impact is $2FC_R$. The mass centre of the shell with mass M_s will simultaneously translate a distance FC_R. Thus the effective dynamic mass of the shell is $M_s^* = M_s/2$, Fig. 4b.

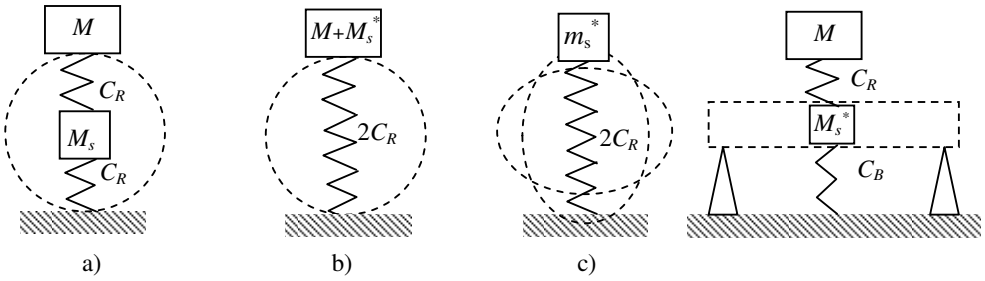

Figure 4: Dynamic masses during deformation of the cylinder cross section.

There is an additional contribution m_s^* to the dynamic mass associated with the deformation of the cross section, Fig. 4c. For a short isotropic cylinder it may be appreciated by equating the frequency ω_{1D} for the one-dimensional vibration of the mass m_s^* at the top of the spring in Fig. 4c with the frequency ω_{2D} [17] for the two-dimensional vibration mode in Fig. 4c:

$$\omega_{1D} = 1\Big/\sqrt{2C_R m_s^*} \Leftrightarrow \omega_{2D} = 2\sqrt{G/\rho}\,/a \;\Rightarrow m_s^* = M_s\Big/\left[12(1-\nu)\left(\pi^2-8\right)\right] \approx M_s/16 \qquad (16)$$

Here G is the shear modulus and ρ is the density. The mass associated with section deformation clearly has a negligible influence on the dynamic mass of the cylinder.

The dynamic mass of a long floor-supported cylinder will be smaller than $M_s/2$ as significant deflections only affect a portion of the total cylinder. In this case it is sufficient to consider a fraction of the total mass, say $M_s^* = M_s L_{zF}/L$, which according to Eq. (5) corresponds to the region where deflections are at least 14% of the peak value.

The deflection of a long end-supported cylinder with central load is:

$$w_B = FC_B \qquad \text{where} \begin{cases} C_B = (2L)^3\Big/\left[48E_z I_x\right] & \text{for simply supported ends} \\ C_B = (2L)^3\Big/\left[192E_z I_x\right] & \text{for clamped ends} \end{cases} \qquad (17)$$

The dynamic mass M_s^* of a long cylinder with simply-supported ends is obtained in the same manner as for Eq. (16) by equating ω_{1D} to the axial bending frequency ω_{2D} [17]:

$$\omega_{1D} = 1\Big/\sqrt{(C_B + C_R)M_s^*} \le 1\Big/\sqrt{C_B M_s^*} \quad \omega_{2D} = \pi^2\sqrt{EI/m}\,\Big/(2L)^2 \Rightarrow M_s^* \le M_s/2 \qquad (18)$$

In conclusion, quasi-static response occurs when the impactor mass is much larger than the dynamic mass of the cylinder. This condition is satisfied by impactors five times heavier than the cylinder, and by lighter impactors for a long tube having floor support.

6. TOTAL DISPLACEMENT AND IMPACT RESPONSE

It is pointed out in [10] that the finite length corrections are based on the assumption that the cylinder length is at least in the order of the radius. A careful study of the results in [10] reveals that the ring solution w_R becomes more compliant than the solution for a finite cylinder with free ends when $L<0.7L_{zF}$. The fact that both solutions impose certain artificial constraints on the deformation, implies that they provide lower bounds on the correct solution. Thus the approach between the point of load application and the centre of a full cylinder with free ends may be approximated as follows:

$$w_F = \begin{cases} w_R & \text{for } L < 0.7L_{zF} \\ w_F & \text{for } L \ge 0.7L_{zF} \end{cases} \qquad (19)$$

The lower part of a floor-supported cylinder with free ends essentially deforms as the lower half of a wide ring under opposite line loads, which has deflection w_R. Thus, the total displacement w_Σ under the load in a floor-supported cylinder with free ends is:

$$w_\Sigma = w_F + w_R + w_D + w_\alpha \tag{20}$$

The centre line of a long cylinder with rigid diaphragms and supports at the ends will deform in bending, with associated deflection w_B. The total displacement under the load in an end supported cylinder with end sections prevented from deforming becomes:

$$w_\Sigma = w_F + w_B + w_D + w_\alpha \tag{21}$$

For curved panels with free ends a lower limit for the deflection is given by a curved shell undergoing cylindrical bending, i.e. the solution for a wide arch. The total displacement in a curved panel with pinned edges and free ends then becomes:

$$w_\Sigma \geq w_P + w_D + w_\alpha \tag{22}$$

The displacements w_i are all expressed in terms of the load and under quasi-static conditions (M_s*<<M) the peak load is easily found by equating the impact energy with the deformation work to peak load:

$$\begin{aligned} &MV_0^2/2 = W_{\max} \qquad \text{where} \quad W_{\max} = \int_0^{w_{\Sigma\max}} F \cdot dw_\Sigma = \int_0^{F_{\max}} F \cdot C_\Sigma(F)\, dF \\ &\text{For linear conditions:} \quad W_{\max} = C_\Sigma F_{\max}^2/2 \qquad \Rightarrow F_{\max} = V_0\sqrt{M/C_\Sigma} = V_0\sqrt{k_\Sigma M} \end{aligned} \tag{23}$$

where $C_\Sigma = dw_\Sigma/dF$ is the total compliance of the system. For linear elastic conditions the quasi-static impact response history is given by:

$$F(t) = F_{\max}\sin\left(\pi \cdot t/T_{imp}\right) \qquad w = C_\Sigma F(t) \qquad \text{where} \quad T_{imp} = \pi\sqrt{MC_\Sigma^*} \tag{24}$$

Here T_{imp} is the impact time and $C_\Sigma^* = 1/k_\Sigma^*$ is the average compliance up to peak load.

7. LOAD AND ENERGY FOR DELAMINATION ONSET

Theory and experiments have demonstrated that the load for delamination growth in plates is independent of the delamination size, and that the delamination threshold load under quasi-static conditions can be expressed as follows for orthotropic plates [8]:

$$\begin{aligned} &F_{d1} = \pi\sqrt{32G_{IIc}D^*/3} \\ &\text{where} \quad D^* = \sqrt{D_{11}D_{22}(1+\eta)/2} \quad \text{and} \quad \eta = (D_{12}+2D_{66})/\sqrt{D_{11}D_{22}} \end{aligned} \tag{25}$$

This expression should also be valid for delamination onset in curved laminates, as the delamination radius initially is negligible in comparison to the radius of shell curvature. However, the assumptions from plate theory will obviously become increasingly invalid during the subsequent growth. Support for a common threshold load can be found in a recent experimental study of impact on flat and curved 3 mm AS4/8552 quasi-isotropic laminates [7]. The delamination load was highly repeatable at about 3.8 kN for convex laminates, 4.9 kN for concave laminates and 5.3 kN for flat laminates impacted by 12.7 mm diameter hemispherical impactors. Assuming a mode II toughness of G_{IIc}=825 J/m^2 [18] and the elastic properties given in [7] the predicted delamination threshold load is 3.5 kN. The higher load for flat and convex laminates can partly be explained by large deflection membrane stiffening [8]. The impact energy required for delamination onset is easily obtained by equating the delamination threshold load with the peak load in Eq. (25).

8. COMPARISON WITH EXPERIMENTS

Predictions based on the suggested approach were compared with results from three available experimental studies [4, 5, 7]. Material properties resulting from the available ply data are listed in Table 1. Ply data for a generic E-glass/epoxy was used since no data was available for the specific material in [5]. Data for the interlaminar toughness G_{IIc} have been taken from the literature, preferably for delamination between non-parallel plies. Toughness data was unavailable for IM7/55A, so the assumed value is based on a typical value for AS4/3501-06, which has similar properties according to [4]. The toughness of E-glass/Epikote 828 refers to interfaces between plain-weave plies of the same material system, which should have a certain similarity with the filament wound material. The geometry and test conditions have been listed in Table 2.

Table 1. Material data for cases considered

Case	Material	Layup	E_z [GPa]	E_θ [GPa]	$\nu_{z\theta}$	G_{IIc} [J/m^2]
[4]	IM7/55A	$[90/\pm22]_2$	52.2	69.9	0.16	525
[5]	E-glass/Epikote 828	$[\pm55]_n$	11.0	19.6	0.36	2064 [19]
[7]	AS4/8552	$[\pm45/0/90]_{3s}$	54.0	54.0	0.3	825 [18]

Table 2. Geometry and test conditions in cases considered

Ref.	$2L$ [mm]	a [mm]	h [mm]	S [mm]	M [kg]	M_s [kg]	L^*/a	Support
[4]	420	49	1.52	tube	5.0	0.4	4.6	Cradled
[5]	500	78	6.00	tube	36.0	2.6	3.7	By floor
[7]	150	132.5	3.00	98	4.5	0.1	0.6	Edges S-S

Figures 5 and 6 illustrate the measured and predicted behaviour for the tubular cylinders in carbon/epoxy tubes in [4] and [5]. Predictions are in good agreement with experiments until the predicted delamination onset, when the stiffness decreases considerably. In Fig. 6 the delamination onset is visible as a dip in the loading curve.

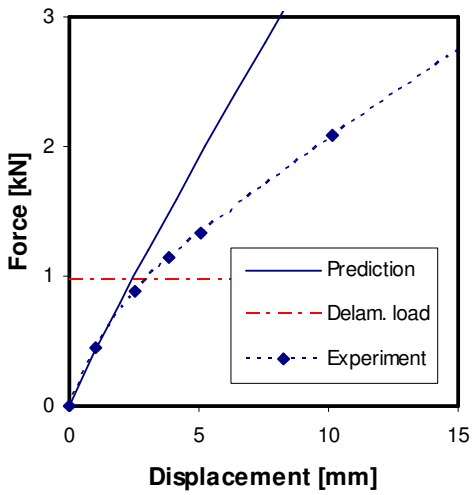

Figure 5: Comparison with experiment by Christoforou et al. on full cylinder [4].

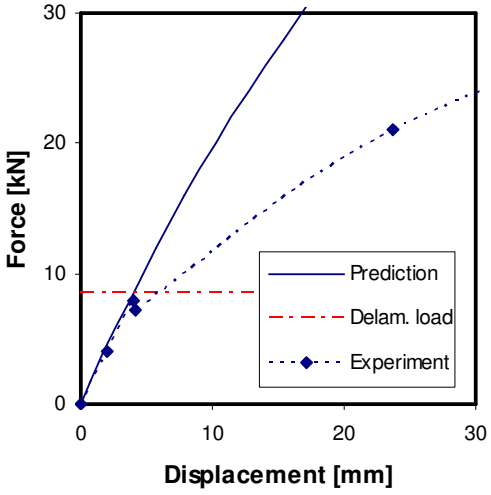

Figure 6: Comparison with experiment by Alderson and Evans on full cylinder [5].

Figure 7 shows the comparison between predicted and measured load versus deflection for a 25 mm diameter indentor impacting the shallow curved carbon/epoxy panels in [7]. The delamination onset is visible as a sudden drop in the load. The nonlinear response prior to delamination onset is significant in this case, and the model is not fully able to capture the nonlinearity observed in the experiment.

Figure 8 shows a comparison between predicted and measured response history during a 13 J impact on the curved panel. The predicted peak load is calculated from Eq. (23), using the nonlinear load-deflection relation, and the response history from Eq. (24) using the linearised compliance C_{Σ}^{*}. A fairly good agreement is seen up to the predicted delamination onset, where the experimental response starts to deviate, as expected.

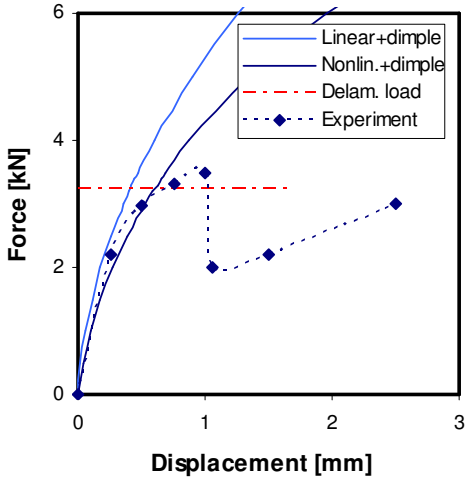

Figure 7: Comparison with experiment by Sun on shallow curved plate [7].

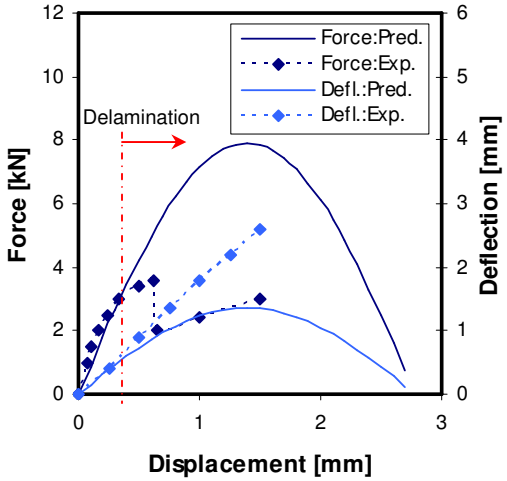

Figure 8: Predicted and measured response history in Sun's experiment [7].

9. DISCUSSION AND CONCLUSIONS

Previous attempts to predict impact response in shells have either been purely numerical (e.g. FE-solutions) or "black box" type analytical solutions based on stepwise numerical solution of lengthy serial expressions. The current paper has presented an alternative approach based on closed form solutions and demonstrated that they can be used to predict response and delamination onset during large mass impact on cylindrical and curved laminates.

The approach is currently limited to events up to the point of delamination onset, and further work should aim to predict the subsequent response and delamination growth, along the lines previously presented for flat plates [8].

Existing models for complete cylinders seem to be satisfactory, while the suggested arch model is limited to relatively short curved panels. Additional work is therefore needed to develop a more general model for curved panels, and to establish the range of validity for the arch model.

The suggested corrections for large deflections are highly simplified. Fairly good agreement was observed for the complete cylinders, while the present model seems unable to fully capture the stiffness reductions caused by large deflections in curved panels. Further studies are required to develop an improved account for large deflection effects under concentrated loads in cylinders, particularly in shallow curved panels.

REFERENCES

1- Davies, G.A.O. and Olsson, R., "Impact on composite structures", *The Aeronautical Journal* 2004;108(1089):541-563.
2- Iannou F. and Olsson, R., *"Simple structural models for impact on curved panels",* Report TR07/08, The Composites Centre, Imperial College, London 2007.
3- Kistler, L.S. and Waas, A.M. "Experiment and analysis on the response of curved laminated composite panels subjected to low velocity impact", *International Journal of Impact Engineering* 1998;21(9):711-736.
4- Christoforou, A.P., Swanson, S.R. and Beckwith, S.W., " Lateral impact of composite cylinders", in *Composite Materials: Fatigue and fracture, 2nd vol.*, ASTM STP 1012, ed. Lagace, P.A., ASTM, Philadelphia 1989:373-386.
5- Alderson, K.L. and Evans, K.E., "Low velocity transverse impact of filament-wound pipes: Part 1. Damage due to static and impact loads", *Composite Structures* 1992;20(1):37-45.
6- Wardle, B.L and Lagace, P.A., "Importance of instability in impact response and damage resistance of composite shells", *AIAA J* 1997;35(2):389-396.
7- Sun, L, "*Curvature effect on impact resistance and damage tolerance of quasi-isotropic panels*", MSc final project report, Department of Aeronautics, Imperial College, London 1997.
8- Olsson R., "Analytical prediction of large mass impact damage in composite laminates", *Composites: Part A* 2001;32(9):1207-1215.
9- Yuan, S.W. and Ting, L., "On radial deflections of a cylinder subjected to equal and opposite concentrated radial loads", *J. of Applied Mechanics* 1957;24(2):278-282.
10- Ting, L., Yuan, S.W., "On radial deflection of a cylinder of finite length with various end conditions", *J. of the Aeronautical Sciences* 1958;24:230-234.
11- Morley, L.S.D., "The thin-walled circular cylinder subject to concentrated radial loads", *Quarterly J. of Mechanics and Applied Mathematics* 1960;13(1)24-37.
12- Jones, I.A., "Approximate solutions to the orthotropic pinched cylinder problem", *Composite Structures* 1998;42(1):73-91.
13- Hedner, G. ed., "*Formelsamling i hållfasthetslära*" 8th edition, Publication 104, Dept of Solid Mechanics, Royal Inst. of Technology, Stockholm 1978.
14- Timoshenko, S.P. and Woinowsky-Krieger, "*Theory of plates and shells*", 2nd edition, McGraw-Hill, New York 1959:501-507.
15- Pogorelov, A.V., "Geometrical methods in the non-linear theory of shells", in "*Theory of thin shells*", Niordson, F.I., ed., Springer Verlag, Berlin 1960:294-300.
16- Biezeno, C.B., "Das Durchschlagen eines schwach gekrümten Stabes", *Zeitschrift für angewandte Mathematik und Physik* 1938;18(1):21-30.
17- Markuš, Š, "*The mechanics of vibrations of cylindrical shells*", Elsevier, Amsterdam 1988.
18- Hiley, M.J., "Delamination between multi-directional ply interfaces in carbon-epoxy composites under static and fatigue loading", *2nd ESIS TC4 Conference on Polymers and Composites*, Les Diablerets, Switzerland, 1999.
19- Thanomsilp, C. and Hogg, P.J., "Interlaminar fracture toughness of hybrid composites based on commingled yarn fabrics", *Composites Science and Technology* 2005; 65(10):1547-1563.